Bulletin of the Seismological Society of America, Vol. 102, No. 1, pp. 309–320, February 2012, doi: 10.1785/0120110065

Contemporary Seismicity in and around the Yakima Fold-and-Thrust Belt in Eastern Washington

by J. Gomberg, B. Sherrod, M. Trautman, E. Burns, and D. Snyder

Abstract We examined characteristics of routinely cataloged seismicity from 1970 to the present in and around the Yakima fold-and-thrust belt (YFTB) in eastern Washington to determine if the characteristics of contemporary seismicity provide clues about regional-scale active tectonics or about more localized, near-surface processes. We employed new structural and hydrologic models of the Columbia River basalts (CRB) and found that one-third to one-half of the cataloged earthquakes occur within the CRB and that these CRB earthquakes exhibit significantly more clustered, and swarmlike, behavior than those outside. These results and inferences from published studies led us to hypothesize that clustered seismicity is likely associated with hydrologic changes in the CRB, which hosts the regional aquifer system. While some general features of the regional groundwater system support this hypothesis, seismicity patterns and mapped long-term changes in groundwater levels and present-day irrigation neither support nor refute it. Regional tectonic processes and crustal-scale structures likely influence the distribution of earthquakes both outside and within the CRB as well. We based this inference on qualitatively assessed alignments between the dominant northwest trends in the geologic structure and the seismicity generally and between specific faults and characteristics of the 2009 Wooded Island swarm and aseismic slip, which is the only cluster studied in detail and the most vigorous since regional monitoring began.

Introduction

In this study we examined seismicity in eastern Washington from 1970 to present, cataloged by the Pacific Northwest Seismic Network (PNSN), particularly its relationship to the regional tectonics and other plausible causative or linked processes. A primary goal was to determine if the distribution and characteristics of contemporary seismicity provides clues about regional-scale tectonics or about more localized, near-surface processes, as well as several more focused regional questions. These questions must be answered for big picture studies that use contemporary seismicity patterns to delineate major block boundaries (e.g., McCaffrey *et al.*, 2007). The occurrence of the vigorous 2009 Wooded Island earthquake swarm beneath the Hanford nuclear reservation (Wicks *et al.*, 2011), the completion of a multidisciplinary geophysical and geological study of the active tectonics of the Yakima fold-and-thrust belt (YFTB) (Blakely *et al.*, 2011), and a heightened interest in the seismic hazard within the Columbia basin (Wong *et al.*, 2008; Yeats, 2009) also motivated this study (Fig. 1). More specifically, while progress has been made constraining the deep-seated, large-scale tectonics, its connection with the contemporary seismicity remains speculative at best. Regional lore suggests swarms occur preferentially in the synclines. Recently both Blakely *et al.* (2011) and Wicks *et al.* (2011) suggest that modern seismicity is a response to active regional deformation and speculate that the Wooded Island earthquake swarm manifests ongoing folding in the YFTB, involving buckling of competent layers and slip along less competent bedding planes of the Columbia River basalts that blanket the region.

Improving our understanding of the earthquake and related hazards that face the inhabitants of the several moderate-sized cities and rural areas of eastern Washington and threaten critical dams and power facilities along the Columbia River and the Hanford nuclear reservation (Fig. 1) also motivated this study. Construction of nuclear power plants at the Hanford nuclear Site began in 1943; by 1972 most of the plants were decommissioned, and since 1987 only one plant remains in operation. Other major activities on the Hanford site since 1987 have focused on understanding and remediation of groundwater contamination and the ongoing construction of the world's largest radioactive material treatment plant.

Data

Geologic Structure

The dominant geologic structure in our study area is the north–south converging YFTB, which consists of a series of

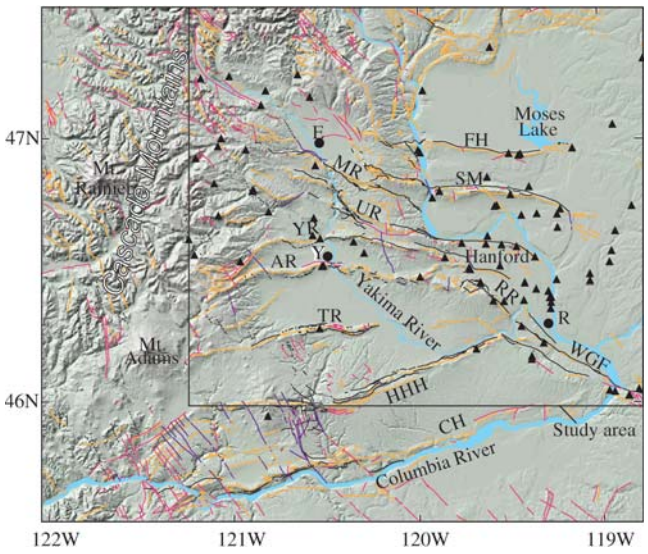

Figure 1. Quaternary faults and fold axes on shaded relief map of eastern Washington and northern Oregon, for the area studied in Blakely *et al.* (2011). Lines show Quaternary thrust (black), normal or concealed dip slip (red), strike-slip (purple), and inferred (dotted) faults and anticline axes (orange) from U.S. Geological Survey Quaternary fault database (U.S. Geological Survey, 2006): FH, Frenchman Hills; SM, Saddle Mountains; UR, Umtanum Ridge; AR, Ahtanum Ridge; RR, Rattlesnake Mountain; MR, Manstas Ridge; YR, Yakima Ridge; TR, Toppenish Ridge; HHH, Horse Heaven Hills; CH, Columbia Hills; WGF, Wallula Gap. The Hanford Nuclear Reservation (labeled) is bounded on the east and north by the Columbia River and was the site of the 2009 Wooded Island swarm (yellow star). Cities indicated by black dots: Y, Yakima; E, Ellensburg; R, Richland. Locations of seismic stations within the study area (dashed box) operated during the study period are shown by black triangles.

east–west and northwest-southeast trending anticlinal ridges and wide synclinal valleys deforming part of the Columbia River basalt group (CRB) (Reidel *et al.*, 1989; Blakely *et al.*, 2011) (Fig. 1). The CRB erupted 17.5–6.0 Ma, covering parts of southeastern Washington, northeastern Oregon, and western Idaho and are believed to be at their thickest (~4 km) in the YFTB region (see Burns *et al.*, 2011; Blakely *et al.*, 2011 and references therein). A basement of Miocene, Oligocene, and Eocene sedimentary rocks (Ohanapecosh, Fifes Peak, and Wenatchee formations) and pre-Tertiary rocks consisting of sedimentary, metamorphic, and granitic rocks underlies the CRB (Reidel *et al.*, 1994; Campbell and Reidel, 1994; Burns *et al.*, 2011). Miocene volcaniclastic and continental sedimentary interbeds are variably found within the flows, and Miocene and more recent fluvial, glacial, and Missoula flood deposits (12–14 ka ago) overlay the CRB (Reidel *et al.*, 2002; Blakely *et al.*, 2011). Regional deformation was probably active prior to and throughout CRB emplacement (Blakely *et al.*, 2011). Numerous faults are found in the YFTB, with reverse faults typically found low on the flanks and bending-moment normal faults on the crests of anticlines (Yeats, 2009). Right-lateral fault offsets of ~150 m and 300–500 m have been measured (Blakely *et al.*, 2011) and strain rates across the YFTB are of the order of 1 mm/yr (McCaffrey *et al.*, 2007), implying earthquake recurrence intervals on individual structures of 10–30 ka (Yeats, 2009).

Surface traces of the major faults and fold axes are taken from the U.S. Geological Survey Quarternary fault database (U.S. Geological Survey, 2006) (Fig. 1). We used a 3D geologic model of the depth to the bedrock beneath the CRB developed by Burns *et al.* (2011) (Fig. 2), constructed for use in a regional numerical groundwater flow study. Data used include stratigraphic interpretations based on more than 13,000 wells and a contiguous compilation of surficial geology and structural features; however, only ~250 wells non-uniformly sample the CRB-bedrock interface, so Burns *et al.* (2011) supplemented the well data with the CRB thickness map of Reidel *et al.* (2002). All these data were simplified and used to construct piecewise-smooth trend surfaces that represent upper and lower subsurface geologic model unit boundaries on a 500-foot grid, with variable uncertainties on the order of 150 m (see fig. 11d of Burns *et al.*, 2011).

Earthquake Catalog

We extracted all earthquakes with $M > 0.0$ in the 1970–2010 catalog compiled by the PNSN (see Data and Resources) within the region 46.0° N to 47.5° N, 121.25° W to 118.75° W, which is the same region examined in Blakely *et al.* (2011). The extracted catalog contains 6911 earthquakes, which we winnowed to 5160 by applying various criteria meant to eliminate the most poorly constrained hypocenters but retained enough data to identify temporal and spatial patterns. Almost 30% of all events occurred after 1 January 2009, with most of these belonging to the Wooded Island swarm (Figs. 1, 2). We did not attempt to relocate any earthquakes because the improvement in accuracy would likely not change our assessments of the seismicity patterns and their correlations with imprecisely known geologic structures and other features. We made mostly qualitative visual comparisons and inferences because of numerous inherent limitations in the catalog and the data it was derived from, described in the following text.

Although undoubtedly an underestimate of the true uncertainty (Gomberg *et al.*, 1990), we used the distance uncertainty estimates listed in the PNSN catalog as a measure of the quality of the hypocentral determinations. The root-mean-square travel-time misfits correlated strongly with the distance uncertainties so either could have been used as a quality metric. We retained catalog entries with misfit values ≤0.3 s, which comprise ~80% of the data and required hypocenters to be derived from at least six phases and a minimum recording distance of ≤20 km, which ensured that the distance uncertainties were less than ~5 km.

As noted in the following text, focal depths are important characteristics for testing hypotheses about what causes earthquakes in eastern Washington. The location procedure used by the PNSN employs a conventional iterative least-squares approach; fixed depths sometimes result, either at meters

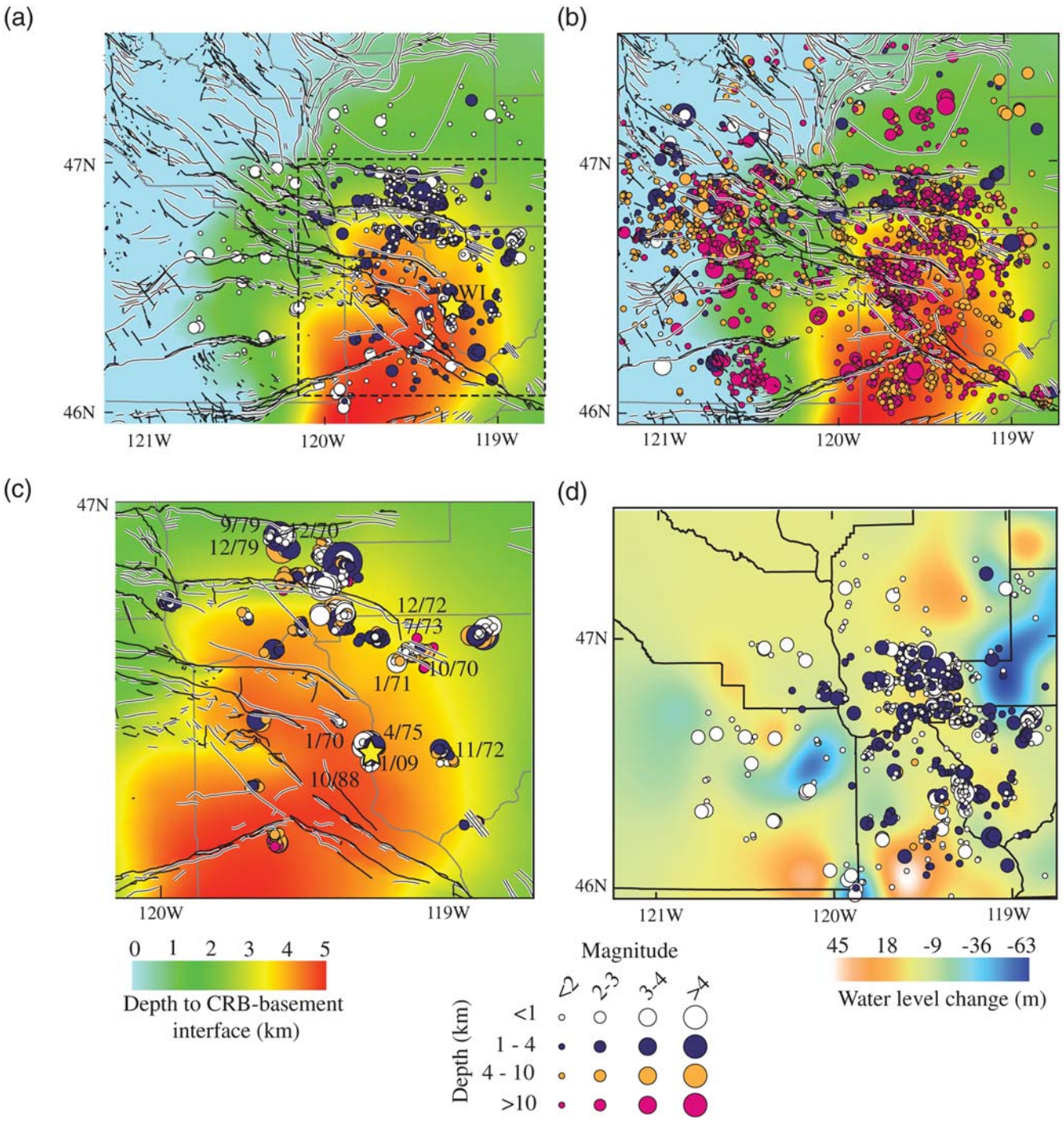

Figure 2. Epicenters, faults and folds, depth to the base of the Columbia River basalts (CRB), and groundwater level changes. (a) Epicenters of cataloged earthquakes (circles) that have focal depths above the base of the CRB, location of the 2009 Wooded Island swarm (yellow star), surface traces of Quaternary faults (black lines) and fold axes (lines with halos) from the U.S. Geological Survey Quaternary fault database (U.S. Geological Survey, 2006), superimposed on the depth to the base of the CRB taken from Burns *et al.* (2011). Gray lines denote county boundaries. (b) Same as (a) but for earthquakes below the CRB. (c) Expanded view of (a) within dashed box but instead of all CRB earthquake epicenters, we show those identified as clusters assuming parameter set 5 in Table 1. For several of the clusters the start dates are noted, illustrating that at some spots the seismicity appears to turn on and off, with hiatuses of months to years. (d) Earthquake epicenters shown in (a) but superimposed on smoothed groundwater level changes between 1984–2009 interpolated from values reported in Snyder and Haynes (2010).

below the surface to avoid solutions above the Earth's surface (28% of the catalog) or after reaching a specified number of iterations without the depth changing significantly (6.5% of the catalog). The large number of depths fixed near the surface suggests that the true depths of those events are probably shallow but indeterminately so, at depths of a few kilometers

or less. Comparisons between higher-accuracy relocated hypocenters and PNSN catalog hypocenters for events within the 2009 Wooded Island swarm (next paragraph) support this suggestion. However, we also considered the more conservative possibility that nothing can be assumed about the depths of these events and performed our analyses assuming the cataloged depth and eliminating all events with focal depths ≤50 m (80% of the fixed depths).

We did not explicitly invoke requirements for *S*-wave arrival time measurements, which can provide strong constraints on focal depth estimates (Gomberg *et al.*, 1990), because this would likely bias the resulting catalog to include preferentially the deeper events and thus would conflict with our objective of examining the spatial distribution of earthquakes. However, for each earthquake the PNSN catalog contains the numbers of stations and phases from which measurements were made, and the difference of these is likely the number of *S*-wave arrival times. For our dataset the mean and median of this number equal 2.0, implying that at least half the hypocenter estimates are constrained by 2 or more *S*-wave arrivals. We further assessed the likely accuracy of the PNSN catalog hypocenters by comparing hypocenters of 875 earthquakes of the Wooded Island swarm that were in both the PNSN catalog and relocated using cross-correlation methods to measure arrival times and the algorithm HypoDD (Waldhauser and Ellsworth, 2000; Wicks *et al.*, 2011; see Data and Resources). Histograms of the depths show that the PNSN estimates are systematically shallower by ~0.7 km than for the relocated hypocenters, in part due to the fixing of depths near the surface in the PNSN catalog noted previously. Moreover, the HypoDD algorithm primarily improves the accuracy of the relative locations and thus the spread in the differences between the two populations of estimates is a more meaningful measure of accuracy. As shown in Figure 3, the distribution of differences is not symmetric (a standard deviation is not appropriate), but qualitatively the spread is less than 1 km.

Low seismicity rates also limit quantitative analyses. Our final catalog corresponds to an overall daily earthquake rate of approximately 0.35, which for example, is approximately 30 times lower than that in southern California (Vidale and Shearer, 2006) if scaled to the size of our study area. We did not eliminate earthquakes below the magnitude of completion, M_c (above which all earthquakes should be detected), because doing so left too few observations to make meaningful inferences. To estimate M_c, we made the standard assumption that the logarithm of the number of earthquakes, $\log[N(M)]$ at a given magnitude should increase linearly with decreasing magnitude until M_c is reached. Over 70% of the cataloged magnitudes are below $M_c = 1.5$, where $\log[N(M)]$ deviates from linearity (Fig. 4). A more liberal approach of eliminating all events with $M < 1.1$, where

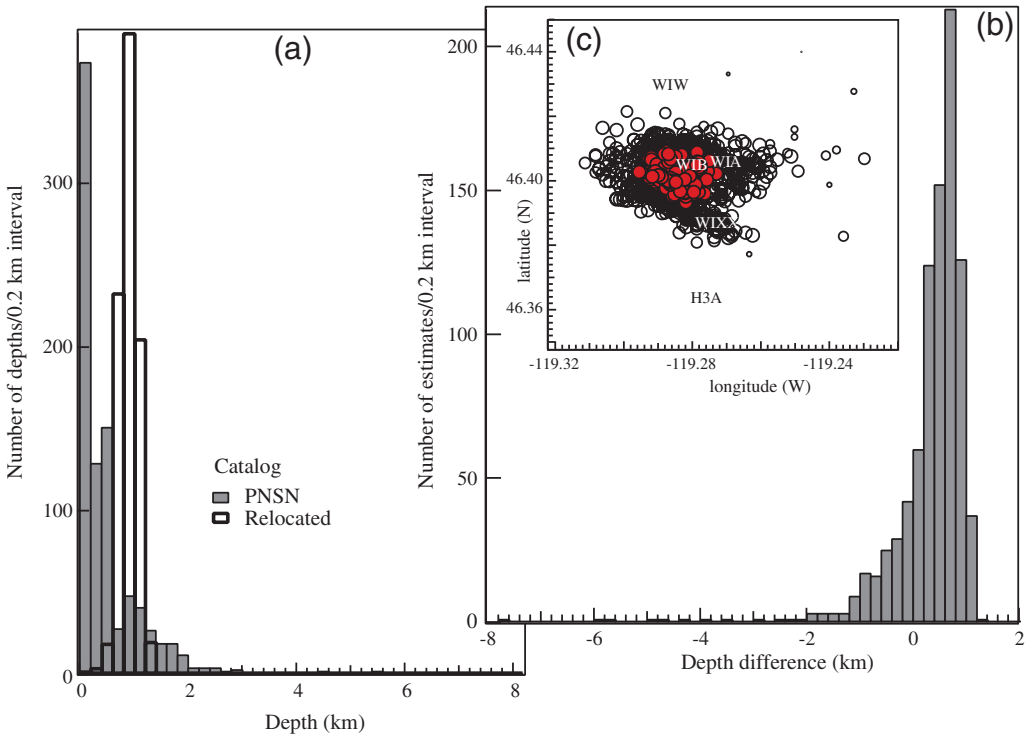

Figure 3. Comparison of Wooded Island swarm PNSN and relocated hypocenters. (a) Histograms of focal depth estimates for 875 earthquakes, derived for the PNSN catalog and relocated for the study of Wicks *et al.* (2011). (b) Histogram of the differences between depths used in (a). (c) Map view of PNSN catalog (open circles) and relocated (red) epicenters for the same earthquakes in (a) and (b). The circle size for PNSN epicenters is scaled to the depth difference (smallest corresponding to largest difference). The epicentral and focal depth differences correlate with one another and the latter are approximately twice as large.

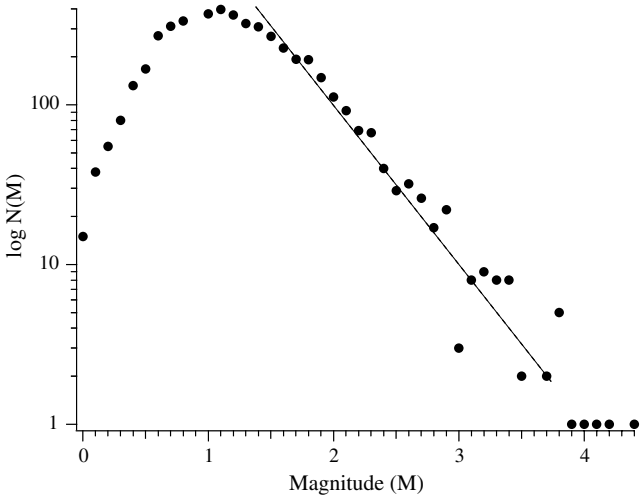

Figure 4. The number of earthquakes versus magnitude for the entire catalog. The dashed line has a slope, or "*b*-value", of one (placed visually). Magnitudes are derived from duration measurements using a relation specific to the PNSN.

log[$N(M)$] peaks, would still reduce the total number of earthquakes by ~42%. These numbers also do not account for the nonuniformity in detection. The present-day level of station coverage was not achieved until 1996, with few stations existing in the western half of the region prior to the mid-1980s. These changes are clearly reflected in the changes in the numbers of earthquakes cataloged in the western half of the study area. The 1996–2008 catalog contains only 23% of the complete catalog, so we examined the entire catalog period but kept in mind the variability in detection in our interpretations.

Eastern Washington Seismicity Analyses and Inferences

Cluster Identification Analysis

A wide variety of approaches have been used to identify and characterize the spatial and temporal patterns of seismicity (see Appendix and references therein). We took a very simple qualitative approach, because the catalog limitations did not permit a meaningful statistical analysis of these patterns. We assessed the degree to which earthquakes may be clustered by asking for each earthquake if there were at least N earthquakes within some specified distance and time and if so, considered all events within this space-time window to be a cluster. We omitted all earthquakes after 1 January 2009 because most of the earthquakes after this date belonged to the Wooded Island swarm. We identified clusters using a suite of temporal and spatial windows, with ranges chosen based on the Wooded Island swarm and a visual inspection of all the seismicity. As expected, more clusters were identified as the windows were increased, and while we report the full range of results, our conclusions do not depend on any specific parameter set. Table 1 summarizes results for all the clustering parameters tested, with $N = 10$ in all cases. To ensure that we were not biased by assumptions made regarding the events with depths that were fixed to stabilize convergence, we repeated the clustering analyses excluding all events with depths ≤50 m and report results in Table 2. Because the clustering results varied monotonically with window size, in this second winnowed suite we only needed to repeat the analysis for the shortest and longest temporal windows to capture the full range of results considered using all the data.

We found the seismicity to be strongly clustered. For the parameter sets tested, the percentage of earthquakes that belong to clusters ranges between extremal values of 19% to 59% with the most reasonable values of the order of 30% or more. In addition, only a small fraction of the clusters have characteristics expected for mainshock–aftershock sequences. Three of the four $M \geq 4.0$ earthquakes in the catalog do not belong to a cluster, for almost all of the clustering parameters chosen; only the largest event belongs to a cluster and has the characteristics expected for a mainshock–aftershock sequence (i.e., the M 4.4 earthquake is the first of tens of earthquakes, all within a specified distance and time interval and with a temporally decreasing rate). If we applied a minimum criteria for a mainshock–aftershock sequence, that the first event in the cluster is the largest, only 8% to 22% of all the clusters identified would be considered potential mainshock–aftershock sequences. In other words, one-third of all the earthquakes in the region are likely clustered, and most of these or more have characteristics more typical of swarms.

Cluster Evolution

The evolution in time and space of clusters of seismicity provides clues about the reactivation of preexisting structures and nature of the loading processes (see Appendix). Visually, smaller clusters themselves appear to cluster, filling areas spanning tens of kilometers over periods of years and suggestive of some process that localizes stress release on scales of a few kilometers over months and migrates a few tens of kilometers over years. We examined this pattern more carefully near the Wooded Island swarm, where two definitive clusters were identified prior and adjacent to the 2009 Wooded Island swarm. These occurred between 15 January 1970 and 29 May 1970 with 18 earthquakes and between 13 April 1975 and 14 August 1975 (Fig. 2c) with 58 earthquakes (assuming parameter set 5). These clusters both would be classified as swarms because the largest events, M 2.3 and M 2.8 earthquakes, respectively, happened in the middle of the sequences and both swarms had hiatuses, lasting 28 and 19 days, respectively. Several tests lead us to conclude that the Wooded Island swarm was not a recurrence in precisely the same place. First, we relocated earthquakes in the 1970 and 1975 swarms using identical procedures as for the cataloged Wooded Island swarm and found systematic shifts by several hundred meters at most, but in the wrong direction or too small to coincide with the Wooded

Table 1

Clustering Parameters and Results*

Parameter Set	Max. Interevent Time (days)	Max. Distance (km)	# of Clusters	# (%) of Events Clustered	# (%) of Clusters with Mainshocks	Cataloged Depths		Randomized Depths	
						# (%) of Events in CRB in Clusters	# (%) of Events below CRB in Clusters	# (%) of Events in CRB in Clusters	# (%) of Events below CRB in Clusters
1	90	4	44	1009 (25%)	7 (16%)	747 (42%)	262 (11%)	501 (29%)	508 (22%)
2	90	8	54	1215 (31%)	11 (20%)	883 (49%)	332 (15%)	608 (35%)	607 (26%)
3	90	16	67	1495 (38%)	11 (16%)	1022 (57%)	473 (21%)	901 (51%)	937 (41%)
4	180	4	48	1146 (29%)	10 (21%)	851 (47%)	295 (13%)	543 (31%)	603 (26%)
5	180	8	54	1372 (35%)	6 (11%)	989 (55%)	383 (17%)	692 (40%)	680 (30%)
6	180	16	79	1838 (46%)	6 (8%)	1198 (67%)	640 (29%)	901 (51%)	937 (41%)
7	270	4	53	1232 (31%)	11 (21%)	902 (50%)	330 (15%)	829 (47%)	852 (38%)
8	270	8	66	1535 (39%)	8 (12%)	1091 (61%)	444 (20%)	787 (45%)	748 (33%)
9	270	16	94	2120 (53%)	14 (15%)	1286 (72%)	834 (37%)	1043 (59%)	1077 (48%)
10	360	4	59	1373 (35%)	11 (19%)	996 (56%)	377 (17%)	691 (39%)	682 (30%)
11	360	8	68	1681 (42%)	14 (21%)	1128 (63%)	553 (25%)	829 (47%)	852 (38%)
12	360	16	103	2369 (59%)	16 (16%)	1377 (77%)	992 (45%)	1160 (66%)	1209 (54%)

*Results of clustering analysis (see text) for 12 different sets of the two free parameters in the analysis, the maximum time (column 2) and distance (column 3) between successive events to consider them part of the same cluster. For each parameter set we note the number of clusters in which the first event is the largest (column 6) and the total number of clustered events for the entire catalog (column 5). The next columns divide this last number into the population within the CRB (column 7) and below the CRB (column 8). The last two columns show this same split, but for analyses in which the populations were randomly selected by first randomizing the depths.

Table 2

Clustering Parameters and Results, Earthquakes with Depth > 50 m*

Parameter Set	Max. Interevent Time (days)	Max. Distance (km)	# of Clusters	# (%) of Events Clustered	# (%) of Clusters with Mainshocks	# (%) of Events in CRB in Clusters	# (%) of Events in CRB in Background	# (%) of Events below CRB in Clusters	# (%) of Events below CRB in Background
1	90	4	31	621 (19%)	5 (16%)	373 (35%)	670 (64%)	248 (11%)	1913 (88%)
2	90	8	37	725 (22%)	5 (14%)	425 (40%)	618 (59%)	300 (13%)	1861 (86%)
3	90	16	45	902 (28%)	4 (9%)	502 (48%)	541 (51%)	400 (18%)	1761 (81%)
10	360	4	45	851 (26%)	9 (20%)	503 (48%)	540 (51%)	348 (16%)	1813 (83%)
11	360	8	55	1117 (35%)	7 (13%)	589 (56%)	454 (43%)	528 (24%)	1633 (75%)
12	360	16	83	1663 (52%)	18 (22%)	745 (71%)	298 (28%)	918 (42%)	1243 (57%)

*The same information as Table 1, but for a catalog in which all earthquakes with focal depths ≤ 50 m were removed, to eliminate data in which depths were fixed at the surface to stabilize the location process.

Island events. Results indicated these hypocentral estimates were sufficiently stable to conclude that they differed from those of the Wooded Island earthquakes, To test the robustness of the locations, we relocated 5 earthquakes in the more poorly constrained 1970 swarm multiple times, each time removing one of the arrival time measurements. Results indicated these hypocentral estimates were sufficiently stable to conclude that they differed from those of the Wooded Island earthquakes; that is, even with fewer measurements, epicenters generally differed $< \sim$1 km and focal depths $< \sim$3 km.

The Wooded Island swarm stands out with respect to the vigor, or rate increase, exhibited anywhere else within or during the study area and time. We conclude that its exceptional nature is probably not an artifact of enhanced detection, although we cannot rule out this possibility for some regions during the early periods of the network's operation. This inference is based on our cluster analysis results (Tables 1, 2) in which we note that, assuming parameter set 5, the highest seismicity rate was 0.93 earthquakes/day for a cluster lasting 28 days in 2000. In contrast, the rate for the first 28 days of the Wooded Island swarm, which does not represent the maximum rate, was 2.2 earthquakes/day. The more than double rate during the Wooded Island swarm is likely not due to differences in detection threshold, because the network configuration was stable by 2000 and no temporary stations had been added yet in the vicinity of Wooded Island.

The CRB, Groundwater, and Seismicity

We tested the hypothesis that a fraction of the seismicity is controlled by groundwater and pore pressure variations by conducting a variety of simple tests. We compared the clustering characteristics between the populations of earthquakes within and below the CRB, which contains the regional aquifer system. Our hypothesis would predict a greater degree of clustering among the population of earthquakes within the CRB relative to that below. We also qualitatively tested for correlations between increased seismicity rates and higher pore pressures by overlaying the earthquake distributions on a contoured map of groundwater changes. This hypothesis was motivated by the observations, particularly the differences in distributions of focal depths of earthquakes belonging to clusters (assuming parameter set 5 in Table 1) and those that do not. We noted that the maximum depth of the CRB is ~4 km and that the depth distribution of the clustered earthquakes peaks at ~3 km and falls off sharply by 5 km (Fig. 5). The depth distribution of the remaining earthquakes is clearly broader, with a significant fraction of depths $>$5 km. A few tens of earthquakes in the clustered population have depths $>$10 km, in contrast to several hundreds in the other population. The depth distribution appears to peak between 0.4 and 0.5 km (Fig. 6) for all three categories of events (freely constrained hypocenters, fixed depths, hypocenters that do not converge), neglecting the peak due to the depths fixed at the surface.

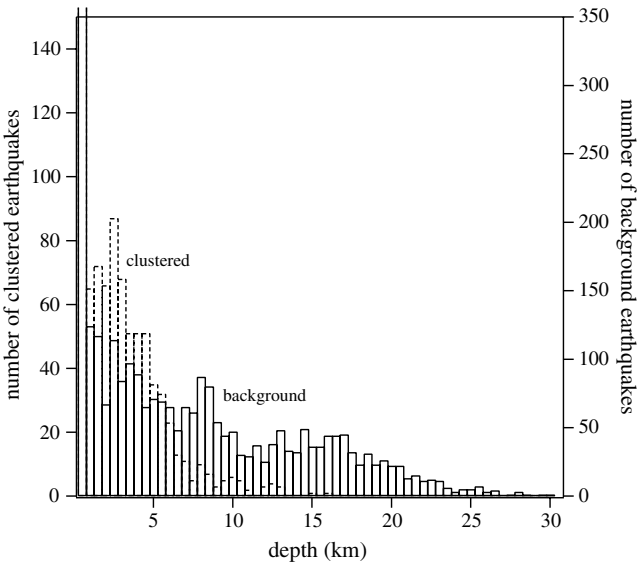

Figure 5. Histograms of the numbers of earthquakes in 0.5 km depth bins, for earthquakes identified as members of clusters (dashed) and not in clusters (solid, labeled "background") using the method to identify both described in the text. To highlight the distributions over the entire depth range, the vertical axis of the nonclustered population has been scaled by 43%, which is the ratio of the number of earthquakes in the clustered and nonclustered populations. Both populations have artificially high numbers of earthquakes with depths $<$0.5 km, because the location procedure fixes depths at the surface to improve convergence in many cases. Thus, the scaling emphasizes depths $>$0.5 km. Results here are for clustering parameter set 5, which defines a cluster as $\geq$10 earthquakes within 180 days and radii of 8 km from the first event in the sequence. The basic features of the distributions remain unchanged for the other parameter sets.

For our quantitative test we used the CRB-bedrock interface model of Burns *et al.* (2011) to sort the earthquakes into two populations. Use of the interface model provides a criterion for sorting in a way that is independent of the observations and relevant to hypothesis testing. We do not draw inferences based on any individual earthquake or cluster, because this sorting into populations is imprecise due to uncertainties in focal depths and the interface model. However, the statistical properties of the populations still provide meaningful insights. We conducted the same clustering analyses for catalogs with and without the earthquakes for which the depths $\leq$50 m, which as noted previously, in almost all cases are constrained during the location process to achieve convergence. The first noteworthy finding is that 26%–52% of the earthquakes occur within the CRB. Another noteworthy finding is that 33%–45% of the earthquakes are within the CRB (the smaller percentage calculated for earthquakes with depths $>$50 m); an additional ~6.6% increase in this range accounts for the uncertainties on the CRB-bedrock interface depth, which is the fraction of all the earthquakes within the 400 m interface depth uncertainty (Burns *et al.*, 2011).

For any given set of clustering parameters the fraction of earthquakes within the CRB that are clustered is a factor

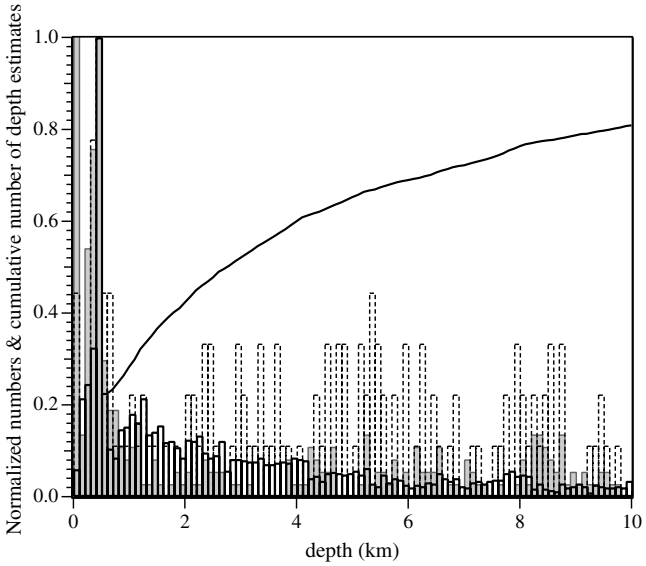

Figure 6. Histograms of focal depths for the populations of earthquakes in which depths were fixed to achieve convergence (shaded), convergence was not achieved (dashed line), and all hypocentral parameters varied until convergence criteria were reached (solid line). The breadth of the second population reflects its small number of total earthquakes (164 out of 5160). All three histograms are normalized to their value in the 0.4–0.5 km bin, which is the maximum for all three populations, neglecting the artificially large number of depths above 0.5 km (resulting from depths being fixed near the surface to achieve convergence). The cumulative number of depths for the population in which convergence was achieved, normalized to its maximum, shows that 50% of the earthquakes have depths <3 km and 75% <8 km (neglecting depths <0.5 km).

of 2 to 3 greater than for the population outside the CRB. Most clusters contain earthquakes both within and below the CRB, but our hypothesis does not require that a single cluster be entirely within the CRB or below. Certainly stresses from tectonic or hydrologic loading and from cluster member earthquakes within one region affect the stresses in another. The percentage of earthquakes in clusters for the population within the CRB ranges from 42% to 77%, which is distinctly higher than the range of 11% to 45% for the earthquakes outside the CRB, with the range corresponding to the most restrictive to inclusive clustering parameters, respectively (Table 1). The result is not significantly different if we consider only earthquakes with depths >50 m; the corresponding ranges are 35% to 71% for the population within the CRB and 11% to 42% for the population outside (Table 2). These distributions of clustering differ significantly from what random chance would predict (last two columns of Table 1). We assessed this by repeating the analyses after randomizing only the depths, because except for 14 earthquakes, all epicenters are within the boundaries of the CRB (i.e., only depths determine whether they are within or outside the CRB). For the randomized populations the percentages of earthquakes in clusters are 29% to 66% for the population within the CRB and indistinguishably different, 22% to 54%, for the population outside.

We attempted to explore the possibility that fluids and pore pressure changes affect seismicity within the CRB by examining the available quantitative data on groundwater changes in the region. Correlations of groundwater fluctuations of ~1 to 20 m with seismicity rates are well documented in the literature (Roeloffs, 1988; Braitenberg, 2000; Saar and Manga, 2003, 2004; Christiansen *et al.*, 2005; Hainzl *et al.*, 2006; Christiansen *et al.*, 2007), particularly with swarm activity (see the Appendix). Such correlations generally are attributed to groundwater recharge (water level increases) due to natural precipitation or to human-generated irrigation, providing natural pore fluid pressure perturbations that can diffuse to depth, decreasing the effective stress, effectively unclamping preexisting faults and triggering earthquakes (Saar and Manga, 2003). Snyder and Haynes (2010) used well data to map water level changes between 1984 and 2009 throughout the Columbia Plateau Regional Aquifer System, which encompasses our study area. They suggested that the region's folds and faults affect groundwater movement by offsetting or altering permeable interflow zones (Drost *et al.*, 1990; Reidel *et al.*, 2002) and estimated that the distances over which flow proceeds unimpeded range between 18 and 64 km. We note that these distances are roughly comparable to the length-scales of the earthquake clusters.

We qualitatively evaluate the hypothesis that seismicity within the CRB should occur more commonly in regions of positive groundwater changes by plotting earthquakes in the CRB on the interpolated and contoured map of groundwater changes of Snyder and Haynes (2010) (Fig. 2d). This assumes that the pattern of groundwater changes measured between 1984 and 2009 represents that from entire period 1970 to 2009 sampled by the seismicity. The net changes in groundwater levels are well in excess of those documented previously, varying spatially by as much as about +45 m and −60 m and dropping generally (due primarily to pumping). However, the rates of groundwater level changes are also important, and those that appear to have triggered seismicity rate increases are of the order of several meters per year, which is comparable only to the extreme average annual rate of 60 m in 25 years. Although speculative only, it is likely that rates exceeded this on shorter timescales. Figure 2d shows that CRB earthquakes appear where the water levels increased, but also in regions where decreases or no clear changes are measured. We show this comparison for completeness, but do not draw any conclusions from it because the groundwater data turn out not to be appropriate for this test.

We also tested our hypothesis by looking qualitatively at several other possible indicators of variations in groundwater, and both also showed no obvious correspondence with the distribution of seismicity. We first searched for a correspondence between areas of higher seismicity rates and irrigated lands. Nearly the entire study region east of the Columbia River has been irrigated since the Columbia Basin Project began delivering river water via its network of canals in 1952. Water flows from the Columbia River at the northern

reaches of the basin toward a reservoir near Moses Lake where it collects and is redistributed to the southern portions of the basin. While the seismicity rate appears to be significantly higher south of Moses Lake, we can think of no physical reason why the direction of flow relative to Moses Lake should affect the seismicity rate. Moreover, the seismicity rate is high southwest of the Columbia River, beyond the reaches of the Columbia Basin Project canal network. We also visually compared the distribution of earthquakes with vegetated areas apparent in Google-Earth imagery, assuming that the latter indicates irrigated lands given the arid climate of eastern Washington. While higher rates of activity occur within pockets of irrigated lands, they also occur where the imagery indicates the land is not vegetated.

Faults, Folds, and Seismicity

As has been noted previously (Wong *et al.*, 2008), our own visual inspection of the distribution of earthquakes, both clusters and background activity, reveals no clear correlations between seismicity and fault traces or fold axes or preferential occurrence for clusters to occur in the synclines (Fig. 2c), contrary to the aforementioned lore about swarms preferentially occurring beneath synclines. However, this lack of correlation is probably not surprising or necessarily meaningful, given that most of the faults dip at uncertain angles and given the uncertainties in earthquake hypocenters. A hint of the same northwesterly trend that dominates the regional faults and folds may be seen in the distribution of earthquakes overall (Fig. 2c,d) and within individual clusters, suggestive of a causal connection. In addition, as noted in the Introduction, features of the Wooded Island swarm and aseismic slip plausibly are causally linked to the Yakima Ridge and other faults imaged in potential field data surrounding the deformation (Blakely *et al.*, 2011).

Discussion

Our investigation results indicate that one-third to one-half of the cataloged earthquakes in eastern Washington since 1970 occur within the CRB, and these CRB earthquakes exhibit significantly greater swarmlike behavior than those beneath the CRB. The only published account of swarmlike activity in eastern Washington prior to the 2009 Wooded Island sequence describes swarms that occurred in late 1972 to early 1974 (Malone *et al.*, 1975). Although precise locations were not reported in Malone *et al.* (1975), epicenters estimated for >100 earthquakes from a temporary network surrounding the swarms concentrated outside and to the northeast and east of the Hanford reservation. Like the Wooded Island earthquakes, focal depths all were shallow, from the surface to just a few kilometers depth. Malone *et al.* (1975) concluded that the earthquakes occurred on multiple faults within the CRB, which was a clear feature of the Wooded Island swarm as well. The activity documented in Malone *et al.* (1975) does not appear in the PNSN catalog.

Starting in January 2009 a swarm of ~1500 earthquakes occurred in the Wooded Island area of the Hanford nuclear site. It is the only earthquake sequence in the region for which geodetic measurements of surface deformation and high-precision earthquake locations are available. Analyses of InSAR data showed that surface deformation resulted dominantly from aseismic slip along a shallow thrust fault (top 2–4 km) and a near-horizontal bedding plane fault of the CRB (Wicks *et al.*, 2011). Blakely *et al.* (2011) suggested that the Wooded Island earthquakes and aseismic slip were caused by flexing of shallow strata associated with movement on underlying, larger structures that form the concealed Yakima Ridge. Notably the geodetic moment of the inferred deformation sources was significantly larger (eight times) than the cumulative seismic moment of the swarm, a feature observed in swarms elsewhere (Roland and McGuire, 2009).

We infer that hydrologic processes may play a role in CRB seismicity based on its greater degree of clustering and previous studies that have correlated clustered and swarmlike seismicity with greater short-wavelength structural heterogeneity, changing and elevated fluid pressures, higher temperatures, sediments, and aseismic deformation transients sometimes initiated or driven by fluid flow (Vidale and Shearer, 2006; Ben-Zion and Lyakhovsky, 2006; Enescu *et al.*, 2009; Roland and McGuire, 2009; Z. Peng, unpublished manuscript, 2010). In addition, the clustering suggests a localization of stress release over distances of 10–30 km or less that persists over decades in some cases, and in some places migrates within these volumes. For example, the map in Figure 2c shows multiple overlapping clusters within areas with radii of ~10 km but separated by decades, as in the region surrounding the 2009 Wooded Island swarm, the very northernmost clusters (clusters in late 1970 and again in 1979), and elsewhere. While alternatives exist, we suggest that fluids migrating through a persistent crack network within the CRB are a plausible source of the aforementioned localized stressing. Wicks *et al.* (2011) suggested that the 2009 Wooded Island deformation event might have been initiated by a pressure pulse caused by changing irrigation practices in the heavily developed agricultural areas surrounding Hanford, or from recent landslides on the bluffs of the nearby Columbia River. While these are plausible explanations for this particular swarm, landslides or direct connections with the Columbia River cannot explain many of the numerous other clusters in the region, which are located far from surficial bodies of water or landslide-prone areas. Our qualitative examinations of seismicity patterns and long-term changes in groundwater levels and present-day irrigation neither support nor refute a hypothesized causal link between seismicity in the CRB and hydrologic changes.

Conclusion

We have examined the characteristics of seismicity in the YFTB that can be gleaned from the PNSN earthquake

catalog between 1970 to present. Our primary goal was to determine if the distribution and characteristics of contemporary seismicity provided clues about the regional-scale active tectonics or about more localized, near-surface processes. We conclude that CRB earthquakes may be controlled by both regional-scale geologic structures and hydrologic processes. The prevalence of clustering within the CRB, relative to the seismicity below, and the characteristics of the clusters provide the primary evidence for a causal connection with hydrologic processes.

We have estimated that between one-half and two-thirds of the earthquakes in eastern Washington occur below the CRB and thus are likely not related to processes confined to the CRB and its interface, but rather to slip on more deep-seated faults responding to regional-scale tectonic deformation. Control provided by regional-scale geologic structure is most clearly suggested for the Wooded Island swarm and associated aseismic slip, which is the only individual swarm with sufficiently well-resolved characteristics to justify inferences about causal connection with geologic structures. Greater precision on both the locations of faults and earthquake sources at depth than are currently available will be required to characterize and understand these relationships.

Data and Resources

All seismic data used in this study were collected and provided by the Pacific Northwest Seismic Network (PNSN). Information about the PNSN and links to its catalog can be found at http://www.pnsn.org (last accessed July 2010). The PNSN catalog used in this study was obtained from the internal archives of the PNSN, and the relocated Wooded Island catalog was obtained from the authors of Wicks *et al.* (2011). All other sources of data are referenced in the text.

Acknowledgments

The authors thank Rick Blakely, David Oppenheimer, and Craig Weaver for their thoughtful and helpful reviews. We are also grateful to the USGS-NAGT undergraduate internship program, which provided support for M. Trautman.

References

Ben-Zion, Y., and V. Lyakhovsky (2006). Analysis of aftershocks in a lithospheric model with seismogenic zone governed by damage rheology, *Geophys. J. Int.* **165,** 197–210.

Blakely, R. J., B. L. Sherrod, C. S. Weaver, and R. E. Wells (2011). Connecting the Yakima fold and thrust belt to active faults in the Puget Lowland, Washington, *J. Geophys. Res.* **116,** doi: 10.1029/2010JB008091.

Braitenberg, C. (2000). Non-random spectral components in the seismicity of NE Italy, *Earth Planet. Sci. Lett.* **179,** 379–390.

Burns, E. R., D. S. Morgan, R. S. Peavler, and S. C. Kahle (2011). Three-dimensional model of the geologic framework for the Columbia Plateau Regional Aquifer System, Idaho, Oregon, and Washington, *U.S. Geol. Surv. Scientific Investigations Rept. 2010-5246*, 44 pp., http://pubs.usgs.gov/sir/2010/5246/ (last accessed February 2011).

Campbell, N. P., and S. P. Reidel (1994). Further exploration for gas warranted in Columbia basin, *Oil and Gas J.*, May, 127–131.

Christiansen, L. B., S. Hurwitz, and S. E. Ingebritsen (2007). Annual modulation of seismicity along the San Andreas Fault near Parkfield, CA, *Geophys. Res. Lett.* **34,** L04306, doi: 10.1029/2006GL028634.

Christiansen, L. B., S. Hurwitz, M. O. Saar, S. E. Ingebritsen, and P. A. Hsieh (2005). Seasonal seismicity at western United States volcanic centers, *Earth Planet. Sci. Lett.* **240,** 307–321.

Drost, B. W., K. J. Whiteman, and J. B. Gonthier (1990). Geologic framework of the Columbia Plateau Aquifer System, Washington, Oregon, and Idaho, *U.S. Geol. Surv. Water-Resources Investigations Rept. 87-4238*, 10 pp., 10 sheets; http://pubs.er.usgs.gov/usgspubs/wri/wri874238 (last accessed June 2010).

Enescu, B., S. Hainzl, and Y. Ben-Zion (2009). Correlations of seismicity patterns in Southern California with surface heat flow data, *Bull. Seismol. Soc. Am.* **99,** 3114–3123.

Gomberg, J., K. Shedlock, and S. Roecker (1990). The effect of *S*-wave arrival times on the accuracy of hypocenter estimation, *Bull. Seismol. Soc. Am.* **80,** 1605–1628.

Hainzl, S., T. Kraft, J. Wassermann, H. Igel, and E. Schmedes (2006). Evidence for rainfall-triggered earthquake activity, *Geophys. Res. Lett.* **33,** L19303, doi: 10.1029/2006GL027642.

Hainzl, S., and Y. Ogata (2005). Detecting fluid signals in seismicity data through statistical earthquake modeling, *J. Geophys. Res.* **110,** 1–10.

Llenos, A. L., J. J. McGuire, and Y. Ogata (2009). Modeling seismic swarms triggered by aseismic transients, *Earth Planet. Sci. Lett.* **281,** 59–69.

Lohman, R. B., and J. J. McGuire (2007). Earthquake swarms driven by aseismic creep in the Salton Trough, California, *J. Geophys. Res.* **112,** 1–10.

Malone, S. D., G. H. Rothe, and S. W. Smith (1975). Details of microearthquake swarms in the Columbia Basin, Washington, *Bull. Seismol. Soc. Am.* **65,** 855–864.

McCaffrey, R., A. Qamar, R. W. King, R. W. Wells, G. Khazaradze, and C. Williams (2007). Deformation in the Pacific Northwest, *Geophys. J. Int.* **169,** 1315–1340.

Mogi, K. (1963). Some discussions on aftershocks, foreshocks, and earthquake swarms: The fracture of a semi-infinite body caused by an inner stress origin and its relation to the earthquake phenomenon, *Bull. Earthquake Res. Inst., Univ. Tokyo* **41,** 615–658.

Ogata, Y. (1992). Detection of precursory relative quiescence before great earthquakes through a statistical model, *J. Geophys. Res.* **97,** 19,845–19,871.

Reidel, S. P., N. P. Campbell, K. R. Fecht, K. A. Lindsey, R. Lasmanis, and E. S. Cheney (1994). Late Cenozoic structure and stratigraphy of south-central Washington, in *Regional Geology of Washington State, Bull. 80*, Washington Department of Natural Resources, Division of Geology and Earth Resources, 159–180.

Reidel, S. P., K. R. Fecht, M. C. Hagood, and T. L. Tolan (1989). The geologic evolution of the central Columbia Plateau, in *Volcanism and tectonism in the Columbia River flood-basalt province, Geol. Soc. Am. Spec. Pap. 239*, S. P. Reidel and P. R. Hooper (Editors), 247–264, Boulder, Colorado.

Reidel, S. P., V. G. Johnson, and F. A. Spane (2002). Natural gas storage in basalt aquifers of the Columbia basin, Pacific Northwest USA: A guide to site characterization, *Pac. Northwest Nat'l Lab. Rep. PNNL-13962*, 277 pp., http://www.pnl.gov/main/publications/external/technical_reports/PNNL-13962.pdf (last accessed June 2010).

Roeloffs, E. A. (1988). Hydrologic precursors to earthquakes: A review, *Pure Appl. Geophys.* **126,** 177–209.

Roland, E., and J. J. McGuire (2009). Earthquake swarms on transform faults, *Geophys. J. Int.* **178,** 1677–1690.

Saar, M. O., and M. Manga (2003). Seismicity induced by seasonal groundwater recharge at Mt. Hood, Oregon, *Earth Planet. Sci. Lett.* **214,** 605–618.

Saar, M. O., and M. Manga (2004). Depth dependence of permeability in the Oregon Cascades inferred from hydrogeologic, thermal, seismic, and

magmatic modeling constraints, *J. Geophys. Res.* **109,** B04204, doi: 10.1029/2003JB002855.

Snyder, D. T., and J. V. Haynes (2010). Groundwater conditions during 2009 and changes in groundwater levels from 1984 to 2009, Columbia Plateau Regional Aquifer System, Washington, Oregon, and Idaho, *U.S. Geol. Surv. Sci. Invest. Rept. 2010-5040*, 12 pp., http://pubs.usgs.gov/sir/2010/5040/ (last accessed June 2010).

U.S. Geological Survey (2006). Quaternary fault and fold database of the United States, from USGS website http://earthquake.usgs.gov/hazards/qfaults (last accessed June 2009).

Utsu, T., Y. Ogata, and R. S. Matsu'ura (1995). The centenary of the Omori formula for a decay law of aftershock activity, *J. Phys. Earth* **43,** 1–33.

Vidale, J. E., and P. M. Shearer (2006). A survey of 71 earthquake bursts across southern California: Exploring the role of pore fluid pressure fluctuations and aseismic slip as drivers, *J. Geophys. Res.* **111,** 1–12.

Waldhauser, F., and W. L. Ellsworth (2000). A double-difference earthquake location algorithm: Method and application to the Northern Hayward Fault, California, *Bull. Seismol. Soc. Am.* **90,** 1353–1368.

Wicks, C., W. Thelen, C. Weaver, J. Gomberg, A. Rohay, and P. Bodin (2011). InSAR observations of aseismic slip associated with an earthquake swarm in the Columbia River flood basalts, *J. Geophys. Res.*, in press.

Wong, I., J. Zachariasen, K. Hanson, B. Swan, R. Youngs, and B. Perkins (2008). Characterization of seismic sources for the probabilistic seismic hazard analyses of the mid-Columbia dams, Draft Report prepared for the *Public Util. Districts of Chelan, Douglas, and Grant Counties*.

Yeats, R. S. (2009). Which Yakima folds are most likely to sustain an earthquake?, *Eos Trans. AGU* **90,** no. 52, Fall Meet. Suppl., Abstract S41F-02.

Appendix

Seismicity Patterns and Clustering in Regions Elsewhere

Seismicity patterns have long been studied to better understand the budgeting and underlying processes of stress build-up and release via rapid slip on faults. In most studies earthquakes are assumed to result from a combination of tectonic loading, from stress changes arising from other earthquakes, and sometimes from nontectonic processes that perturb the stress field (e.g., mining, irrigation, rainfall, etc.). The time-varying rate of seismicity, $\lambda(t)$, triggered by a mainshock of magnitude M_m that occurs at time t_m is often modeled by an equation of the form

$$\lambda(t) = K[(t - t_m) + c]^{-p} \exp[\alpha(M_m - M_{\min})] \qquad \text{(A1)}$$

(see Utsu *et al.*, 1995). Parameters K, c, p, and α are empirical and assumed to be properties of the region, and $M_{\min}$ is the smallest magnitude in the catalog. Equation (A1) shows that the frequency of aftershocks increases with the magnitude of the mainshock and decreases with time after the event.

The stress-transfer from an earthquake also decays with distance from the hypocenter, such that the spatial region in which the subsequent seismicity rate experiences a transient increase scales with the length of the fault that ruptured. In most cases this increase is readily detectable within a distance range comparable to a few rupture lengths, and typically referred to as the aftershock zone. For typical mainshock–aftershock behavior, parameter α in equation (A1) ranges between 1.2 and 3.1 and $p \sim 1$ (Ogata, 1992). However, while still clustered, earthquake-earthquake stress-transfer sometimes appears either less important or predictable and may be characterized as swarms. In these the temporal and spatial developments of the cluster appear independent of the magnitude of its members, such that the sequence does not begin with the single largest event or an abrupt rate increase that monotonically decreases. Hainzl and Ogata (2005), Ogata (1992), and Enescu *et al.* (2009) all characterized bursts of activity using the parameterization of equation (A1) and found consistently lower α values for swarmlike activity (e.g., 0.35 to 0.85 relative to nonswarm values of 1.2 to 3.1), implying lesser dependence of aftershock activity on the mainshock magnitude.

Southern California has been a popular place to study seismicity patterns, presumably because of the high activity rates and availability of high-precision earthquake catalogs. Vidale and Shearer (2006) conducted one of the first studies focused on bursts there, which they defined as an increased rate of earthquakes striking in a limited time and space. They noted that only 20% of bursts exhibited classic mainshock–aftershock characteristics (i.e., the first event being the largest, followed by a decreasing seismicity rate), with the others being more swarmlike. Z. Peng (unpublished manuscript, 2010) used different criteria to identify clusters of increased activity and found that ~57% of these might be considered mainshock–aftershock sequences.

Both Z. Peng (unpublished manuscript, 2010) and Vidale and Shearer (2006) found that classic mainshock–aftershock sequences tended to have thrust-type focal mechanisms, greater depths, and locate in regions of low heat flow. They and Enescu *et al.* (2009) all found that swarms are often associated with high heat flow regions, strike-slip to normal faulting environments, and shallower depths. Vidale and Shearer (2006) suggested that pore fluid pressure fluctuations likely drive swarmlike sequences, but noted that aseismic slip may also be responsible. Z. Peng, unpublished manuscript (2010) inferred that with increasing depth and in regions more favorable for thrust faulting normal stress and crack closure increase, decreasing small-scale heterogeneities and swarmlike activity. Enescu *et al.* (2009) explained swarm activity in terms of a viscoelastic damage rheology model (Ben-Zion and Lyakhovsky, 2006), which predicts that conditions that reduce material viscosity also reduce mainshock–aftershock behavior; conditions may include high temperature and fluid content, and the presence of thick sediments. Correlations of swarms with high heat flow, particularly in geothermal areas, have long been made (Mogi, 1963).

Most studies outside California have concluded that external, often geodetically observable, deformation drives

swarm activity. Lohman and McGuire (2007) and Roland and McGuire (2009) studied swarms on transform boundary fault systems and found unique, distinctive characteristics common to them all include particularly high migration rates and low effective stress drops. These and geodetic observations in a few cases, led them to conclude that swarms are driven by shallow, aseismic, fault slip. Llenos *et al.* (2009) examined four earthquake swarms for which geodetic data were available and linked swarm activity with changes in stressing rate. However, Hainzl and Ogata (2005) reached quite different conclusions and inferred that fluids and pore pressure changes likely initiated the swarms they studied but only a few percent were driven by pore pressure changes, with most resulting from earthquake-generated stress triggering (i.e., cascading activity).

U.S. Geological Survey
University of Washington
Box 351310
Seattle, Washington 98195
(J.G., B.S.)

University of Texas
Geological Sciences
Austin, Texas 78705-2461
(M.T.)

U.S. Geological Survey
Oregon Water Science Center
2130 SW 5th Ave.
Portland, Oregon 97201
(E.B., D.S.)

Manuscript received 1 March 2011